AGU PUBLICATIONS

Geophysical Research Letters

RESEARCH LETTER
10.1002/2017GL072977

Key Points:
- Northwestern shelf sediments record major shifts in Australian climate at 5.5, 3.3, and 2.4 Ma
- We interpret NGR-derived proxies as changes in terrestrial climate from annually to seasonally wet
- Neogene Australian climate is defined by the progressive restriction of ITF by the Maritime Continent

Supporting Information:
- Supporting Information S1

Correspondence to:
B. A. Christensen,
christensen@adelphi.edu

Citation:
Christensen, B. A., et al. (2017), Indonesian Throughflow drove Australian climate from humid Pliocene to arid Pleistocene, *Geophys. Res. Lett.*, *44*, doi:10.1002/2017GL072977.

Received 8 FEB 2017
Accepted 19 JUN 2017
Accepted article online 22 JUN 2017

Indonesian Throughflow drove Australian climate from humid Pliocene to arid Pleistocene

Beth A. Christensen[1], Willem Renema[2], Jorijntje Henderiks[3], David De Vleeschouwer[4], Jeroen Groeneveld[4], Isla S. Castañeda[5], Lars Reuning[6], Kara Bogus[7], Gerald Auer[8], Takeshige Ishiwa[9,10], Cecilia M. McHugh[11], Stephen J. Gallagher[12], Craig S. Fulthorpe[13], and IODP Expedition 356 Scientists[14]

[1]Environmental Studies Program, Adelphi University, Garden City, New York, USA, [2]Naturalis Biodiversity Center, Leiden, Netherlands, [3]Department of Earth Sciences, Uppsala University, Uppsala, Sweden, [4]MARUM-Center for Marine and Environmental Sciences and Department of Geosciences, University of Bremen, Bremen, Germany, [5]Department of Geosciences, University of Massachusetts at Amherst, Amherst, Massachusetts, USA, [6]Energy and Mineral Resources Group, Geological Institute RWTH, Aachen University, Aachen, Germany, [7]International Ocean Discovery Program, Texas A&M University, College Station, Texas, USA, [8]Institute of Earth Sciences, University of Graz, Graz, Austria, [9]Atmosphere and Ocean Research Institute, University of Tokyo, Chiba, Japan, [10]National Institute of Polar Research, Tokyo, Japan, [11]School of Earth and Environmental Sciences, Queens College (C.U.N.Y.), Flushing, New York, USA, [12]School of Earth Sciences, University of Melbourne, Melbourne, Victoria, Australia, [13]Institute for Geophysics, Jackson School of Geosciences, University of Texas at Austin, Austin, Texas, USA, [14]See Section A2

Abstract Late Miocene to mid-Pleistocene sedimentary proxy records reveal that northwest Australia underwent an abrupt transition from dry to humid climate conditions at 5.5 million years (Ma), likely receiving year-round rainfall, but after ~3.3 Ma, climate shifted toward an increasingly seasonal precipitation regime. The progressive constriction of the Indonesian Throughflow likely decreased continental humidity and transferred control of northwest Australian climate from the Pacific to the Indian Ocean, leading to drier conditions punctuated by monsoonal precipitation. The northwest dust pathway and fully established seasonal and orbitally controlled precipitation were in place by ~2.4 Ma, well after the intensification of Northern Hemisphere glaciation. The transition from humid to arid conditions was driven by changes in Pacific and Indian Ocean circulation and regional atmospheric moisture transport, influenced by the emerging Maritime Continent. We conclude that the Maritime Continent is the switchboard modulating teleconnections between tropical and high-latitude climate systems.

Plain Language Summary Australia is the most arid habitable continent on earth, however its climate is capable of dramatic change with seasonal monsoon rains in the otherwise arid northwest. We analyzed natural gamma radiation in a recently drilled borehole (IODP Expedition 356 Site U1463) off NW Australia to examine long-term climate changes over the last 6 million years. Based on variations in potassium, thorium and uranium, as well as common clay minerals, we show that the NW continent was more humid during the Pliocene period, between ~5.5 and 3.3 million years ago (Humid Interval), and became arid by the early Pleistocene, ~2.4 million years ago (Arid Interval). We attribute the Humid Interval to an expansion of warm surface waters in the western Pacific, supplying warm and moist air to the continent. As Australia moved north, the Maritime Continent (islands to the north) emerged, restricting the flow of warm surface currents from the Pacific (Indonesian Throughflow), resulting in drier conditions on land. The Arid Interval ushered in a modern-like Australian climate, with seasonal rainfall and dust storms, and a more modern Indian Ocean circulation. Our results show that the Maritime Continent is an important control on both Australian climate and Indian Ocean circulation.

1. Introduction

The Indonesian Throughflow (ITF) is the only tropical pathway in modern ocean circulation that allows for interbasin transport of warm waters from the western Pacific into the eastern Indian Ocean [*Gordon*, 2005; *Du and Qu*, 2010] (Figure 1). Rainfall on the Maritime Continent and adjacent land masses combined with continental riverine input from areas impacted by the Asian monsoon produces fresher ITF outflow waters [*Molnar and Cronin*, 2015]. Modeling studies show that complete closure of the ITF would significantly reduce moisture availability in northern Australia [*Krebs et al.*, 2011] demonstrating the pivotal role of the ITF for moisture supply to northwest Australia [*Molnar and Cronin*, 2015; *Cane and Molnar*, 2001].

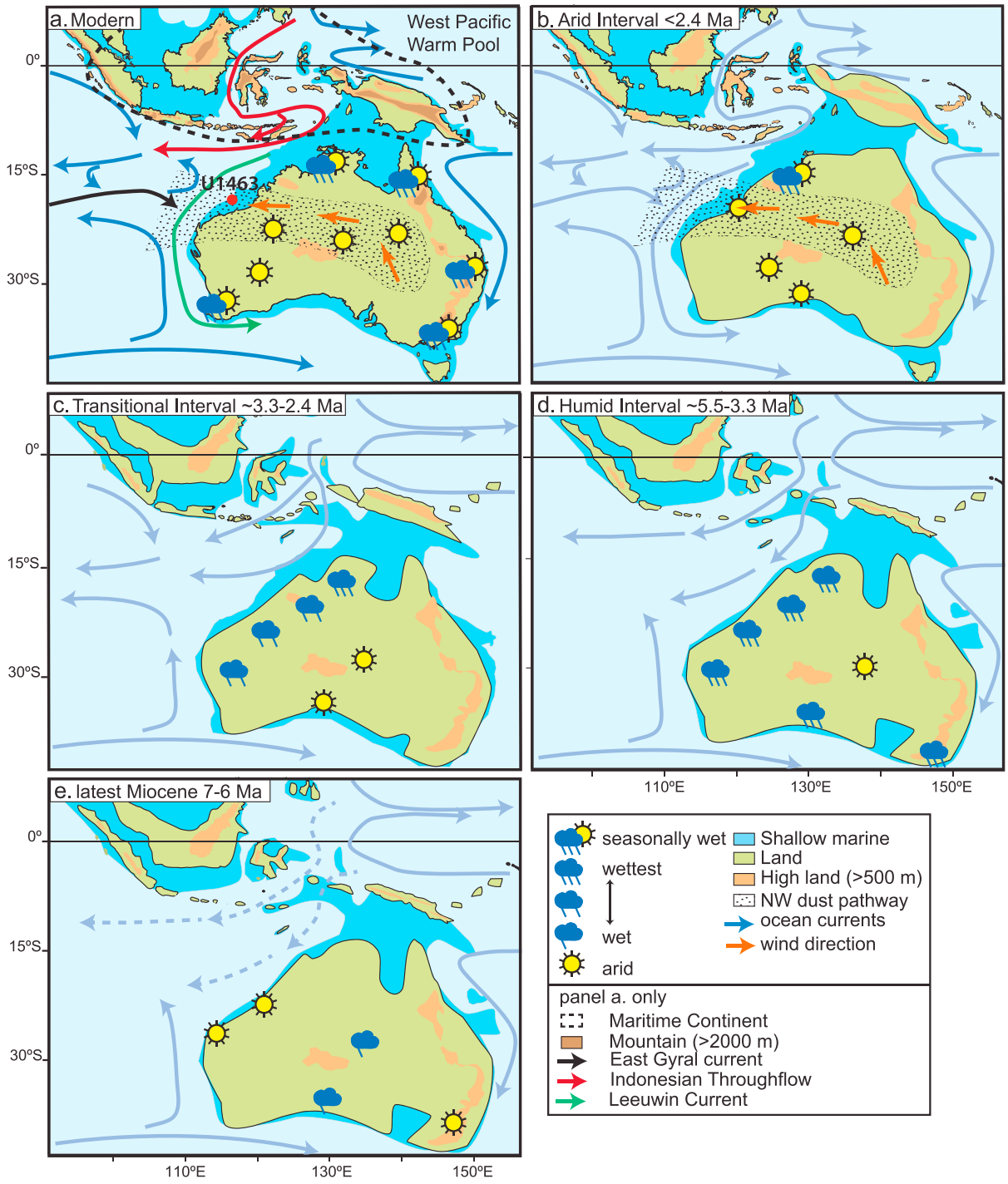

Figure 1. Tectonic and oceanographic change at major periods of Australian Neogene climatic change. (a) Modern setting, Site U1463 location on the northwest Australian shelf; (b) Arid Interval (~2.4 Ma onward); (c) Transitional Interval (~3.3–2.4 Ma); (d) Humid Interval (~5.5–3.3 Ma); and (e) Late Miocene (~7–6 Ma). Paleogeographic maps modified from *Hall* [2012] except Figure 1e which retains the Figure 1d configuration. Modern NW dust pathway in Figures 1a and 1b is after *Bowler* [1976, 1982]. Stylized modern ITF is in red (Figure 1a); East Gyral Current in black; and Leeuwin Current in green; see Figure S1e for detailed circulation patterns.

Today, the austral summer monsoon eases aridity in northwest Australia and is driven by continental heating, with moisture provided by warm Indonesian and western Pacific waters via the ITF (Text S1 and Figure S1 in the supporting information). However, rainfall intensity and temperature are changing with global warming. Extreme events, such as intense rainfall or drought, impact freshwater availability and

distribution, posing societal and economic challenges [*Holper*, 2011; *Hope et al.*, 2010]. Forecasting climate variability and constraining the likelihood of extreme events requires an improved understanding of the fundamental controls on Australian climate, including Indian Ocean circulation and the Australasian monsoon [*Steinke et al.*, 2014].

Over geological time scales, Australia experienced extreme hydrological fluctuations during the late Neogene [*Martin*, 2006; *Groeneveld et al.*, 2017]. Although these changes are likely related to the uplift of the Maritime Continent and subsequent changes in the ITF [*Molnar and Cronin*, 2015], both the timing and controls on Neogene Australian continental climate remain undefined. Our understanding of the mechanisms driving Australian continental aridity and constraints on the rate of paleoclimate change are limited by the absence of long, continuous climate archives on land and offshore. International Ocean Discovery Program (IODP) Expedition 356 [*Gallagher et al.*, 2017] recently drilled sediments on the northwest Australian shelf (Figure 1a), providing robust temporal constraints on Neogene climate. Here we present new climate records from IODP Site U1463 (Figure 2) detailing the timing and magnitude of variability since 5.5 Ma (latest Miocene to Pleistocene) in a regional and global context. While the climate drivers underpinning our long-term records may operate on a different time scale than short-term global change, they have the potential to elucidate the main controls and feedbacks on Australia's complex climate evolution [*Steinke et al.*, 2014; *Fitzsimmons et al.*, 2013].

2. Materials and Methods

2.1. IODP Site U1463 Sedimentology and Natural Gamma Radiation

Sediment recovery at Site U1463 (18°58′S, 117°37′E; 145 m water depth) was 80% [*Gallagher et al.*, 2017], permitting an excellent correlation between the lithology and the downhole wireline logs (Figure S2). Logging data do not include the upper 72 m because the drill pipe was positioned at that depth. Hemipelagic sediments accumulated at rates averaging 6 cm/ky in the Pliocene and 11 cm/ky in the early Pleistocene (Figure S4), allowing for a detailed analysis of continental climate. Sediments are mainly composed of olive gray mudstone and are remarkably homogeneous throughout the studied section. Paleodepth estimates from benthic foraminifera indicate an outer shelf to upper bathyal marine environment (250–1000 m). Sediments used here are from the interval 89.70–413.68 cored meters below seafloor (m CSF-A), corresponding to 88–411 wireline matched below seafloor (m WMSF) and equivalent to Cores U1463B-10H to 48X (Figure S2). The relative content of clay mineral phases (illite and kaolinite) in 17 bulk samples was analyzed using X-ray diffraction (XRD) to ground truth the wireline logs (Text S2).

The Hostile Environment Natural Gamma Ray Sonde (HNGS) was used to measure natural gamma radiation (NGR) in the sediments. The HNGS uses two bismuth germanate scintillation detectors and five-window spectroscopy to determine concentrations of potassium (K, in weight percent [wt %]), thorium (Th, in parts per million [ppm]), and uranium (U, ppm) from the characteristic gamma ray energies of isotopes in the ^{40}K, ^{232}Th, and ^{238}U radioactive decay series (Text S2). The computation of the elemental abundances uses a least squares method of extracting U, Th, and K elemental concentrations from the spectral measurements and is supported by discrete analyses [*De Vleeschouwer et al.*, 2017]. The HNGS filters out gamma ray energies below 500 keV, eliminating sensitivity to bentonite or KCl in the drilling mud and improving accuracy. As the HNGS response is influenced by the borehole diameter, data are corrected for borehole diameter variations. In the upper ~80 m, the HNGS measures NGR through the drill pipe, causing an attenuated signal [*Gallagher et al.*, 2017]. Although relative variations in this interval are meaningful, we do not interpret this portion of the record.

We interpret variations in the concentration of U, Th, and K and the ratio of Th/K as reflecting windblown or riverine flux of detrital material in the marine system. It is possible that some variation could be driven by changes in carbonate production. For example, under a constant flux of detrital (K-bearing) material, a doubling of the sedimentation rate would imply a halving of the K concentration. However, this mechanism is unlikely to be the driver of the K variations at Site U1463 because it would require unusual sedimentation patterns (see section 3.1). We evaluated this issue quantitatively (Figure S5), calculating K, Th, and U flux (Φ, in g/cm^2/kyr) using the following equation:

$$\Phi i = wi^* \rho^* \text{ sed rate},$$

where w is the element i (K, Th, or U) mass fraction, ρ the average bulk density in an interval ± 10 m

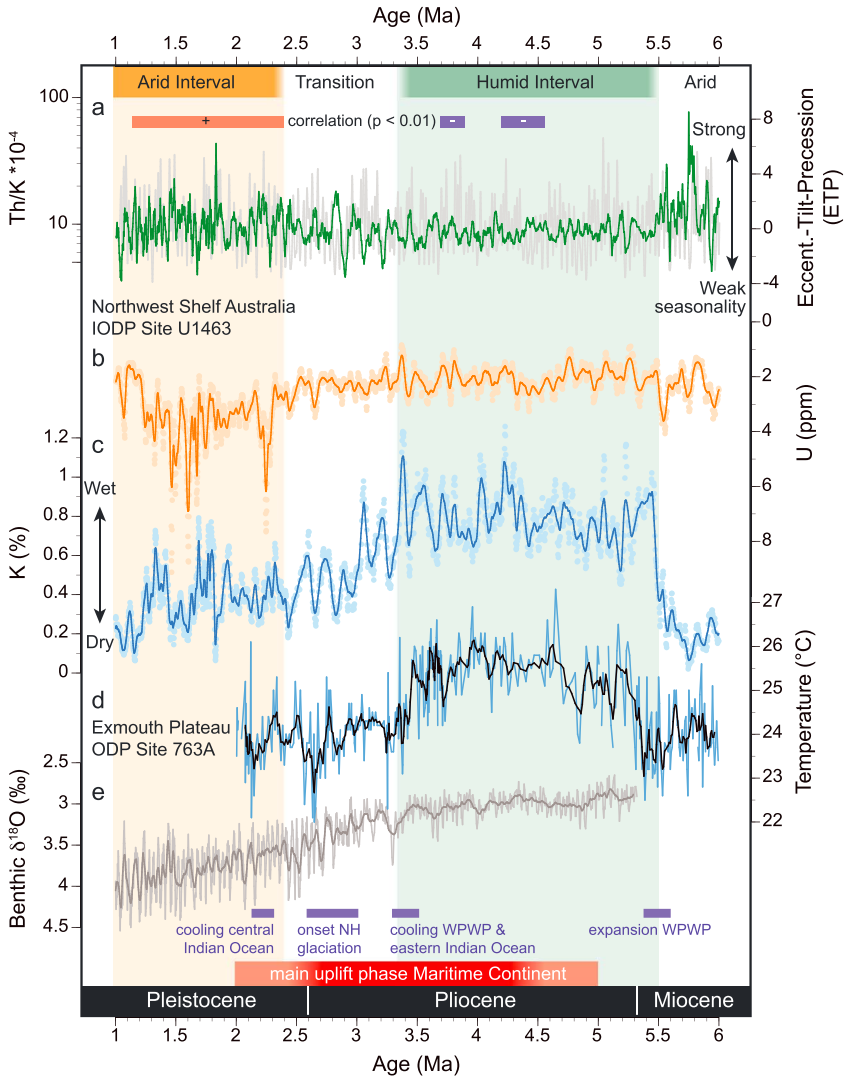

Figure 2. IODP Site U1463 downhole wireline log data plotted by age. (a) Thorium-potassium ratio (Th/K $\times 10^{-4}$), compared to an austral eccentricity-tilt-precession composite. Intervals with significant correlation between both records ($p < 0.01$; 500 kyr windows) are indicated by rectangles (red: positive correlation; blue: negative correlation). Negative correlation indicates enhanced summer precipitation (high %K and low Th/K) at times of relatively high summer insolation (high ETP). (b) Uranium (U ppm) and (c) potassium (%K); lines are 15-point moving average. Note reversed *y* axis in Figure 2b. (d) Mg/Ca-derived temperature records from nearby Site 763A [*Karas et al.*, 2011b] are shown for comparison along with (e) the LR04 benthic foraminiferal stable isotope stack [*Lisiecki and Raymo*, 2005], the Humid Interval (~5.5–3.3 Ma), Transitional Interval (3.3–2.4 Ma), and the Arid Interval (~2.4 Ma onward) are indicated. Blue areas mark major changes in the Western Pacific Warm Pool (WPWP), Indian Ocean circulation, and Northern Hemisphere (NH) glaciation. Uplift in the Maritime Continent (MC), controlling flow through the ITF, is highlighted in red (strongest colors keyed to most likely timing).

surrounding the stratigraphic position in question (in g/cm^3) and *sed rate* the instantaneous sedimentation rate at that position (in cm/kyr).

2.2. Age Model

Site U1463 yielded a complete stratigraphic succession from the late Miocene to the early Pleistocene, with abundant and well-preserved calcareous nannofossils and planktonic foraminifers. The standard zonal

schemes and datums are calibrated to the geological time scale of *Gradstein et al.* [2012]. The depth scale of wireline logs (m WMSF) generally has a small offset from the cored depth scale (m CSF-A), along which the biostratigraphic datums are reported. The offset ranges between 0 and 6.14 m in Hole U1463C, which is the hole in which most biostratigraphic datums were defined. We converted the CSF-A depths of biostratigraphic datums to the WMSF depth scale by correlating distinct features in the wireline and core-based total natural gamma radiation (NGR) records (Figure S2), and linear interpolation between the established tiepoints between the core data and wireline logs. Subsequently, a biostratigraphic age model was constructed for the wireline records by fitting a third-order polynomial through the biostratigraphic tiepoints (Figure S4).

Next, the wireline potassium (K) record was subjected to evolutive harmonic analysis using the 3-2π multitaper method [*Thomson*, 1982], as implemented in the R-package astrochron [*Meyers*, 2014], to detect a possible imprint of astronomical climate forcing (Figure S3). The Site U1463 biostratigraphic age model appears to estimate sedimentation rate accurately throughout the studied interval, as high spectral amplitude is observed at frequencies close to the expected frequencies of eccentricity (100 kyr and 405 kyr periodicity). The 405 kyr eccentricity cycle especially has high amplitude throughout the entire interval. The biostratigraphic age model was then further constrained by applying a cyclostratigraphic approach. We used a band-pass filter (300–500 kyr) to extract variations in K concentrations that are related to the 405 kyr eccentricity cycle. The band-pass filtered signal was then correlated to the La2010 eccentricity solution [*Laskar et al.*, 2011]. This correlation implied only a modest modification of the original biostratigraphic age model, suggesting age shifts of less than a few tens of thousands of years. Only small modifications were expected, as the biostratigraphic age model in the studied interval is well constrained (Figure S4).

We compare the Th/K ratio to an eccentricity-tilt-precession (ETP) composite with equal weight of the three astronomical parameters [*Imbrie*, 1985] (Figure 2a). We use ETP rather than a local insolation signal because ETP exhibits a direct eccentricity imprint. ETP is enhanced under high obliquity (tilt, T), leading to globally increased seasonality. Precession's contribution is positive when perihelion occurs during the austral summer half year, and vice versa, and therefore, maximum of ETP corresponds to maximum in seasonality in the Southern Hemisphere. The Pearson's linear correlation coefficient and associated *p* value are calculated, considering Th/K ratios and their corresponding ETP value within 500 kyr wide windows.

2.3. Organic Geochemistry

Eighteen sediment samples for organic geochemistry were analyzed at the University of Massachusetts Amherst on an aliquot of the squeezecake sediment from shipboard interstitial water sampling, obtained by squeezing 5 or 10 cm whole-round sections [*Manheim and Sayles*, 1974]. Freeze-dried sediments were homogenized and extracted with 9:1 dichloromethane (DCM)/methanol (*v*/v) using an Accelerated Solvent Extractor (ASE 200), and the total lipid extract was separated into apolar (9:1 hexane/DCM (*v*/v)), ketone (1:1 hexane/DCM (*v*/v)), and polar (1:1 DCM/methanol (*v*/v)) fractions using alumina oxide column chromatography. The polar fractions were dissolved in a mixture of 99:1 hexane/isopropanol (*v*/v) and filtered through a 0.45 μm PTFE filter before being analyzed on an Agilent 1260 high-performance liquid chromatography coupled to an Agilent 6120 MSD following the methods of *Hopmans et al.* [2000] and *Schouten et al.* [2002]. TEX_{86} ratios were calculated as described by *Schouten et al.* [2002], and the BAYSPAR calibration [*Tierney and Tingley*, 2014] was applied to derive overall trends in temperature.

3. Results

3.1. NGR as a Proxy for Continental Humidity

The primary data set for assessing moisture and aridity is the natural gamma ray suite of downhole logs, mainly potassium (K) and thorium (Th). The K component of the natural gamma ray log is often used to infer the concentration of K-bearing aluminosilicates, mainly clays and feldspars [*Ehrenberg and Svana*, 2001]. Recently, the abundance of K, normalized to Ca, in marine sediments has been used as a proxy for river runoff and terrigenous input from the northwest Australian continent [*Kuhnt et al.*, 2015]. The covariation of illite with K at Site U1463 supports this relationship (Figure S5). Therefore %K provides an indicator of continental moisture and is consistent with elevated modern %K in association with area watersheds (Figure S6).

Our analyses indicate that the changes in %K are not the result of dilution. For the meter-scale oscillations in the K record between 0.5 and 1 wt % throughout the Pliocene to result from changing sedimentation rates

under a constant flux, the sedimentation rate would have to double and halve in an alternating fashion. Additionally, the Pliocene evolution of sedimentation rates, as estimated by nannofossil and planktonic foraminifera datums, does not correlate with observed changes in %K. The biostratigraphic time constraints suggest overall high sedimentation rate throughout the late Miocene-Pliocene with a relative increase during the early Pleistocene (Figure S4). Finally, the significant intervals of elemental change (Figure 2), which we interpret as climatic change, correspond with changes in flux rather than sedimentation rate (Figure S5).

The Th/K ratio derived from spectral gamma ray logging is a proxy for heavy mineral concentration in the siliciclastic mineral fraction [*Šimíček and Bábek*, 2015]. This relationship is driven by a significant component of heavy minerals, particularly zircon ($ZrSiO_4$), which are associated with Th and U [*Svendsen and Hartley*, 2001] (Text S2). Given this association, and as the abundance of zircon grains is a proxy common for windblown material from the Australian desert [*Simicek and Bàbek*, 2015; *Stuut et al.*, 2014], the Th/K ratio (Figure 2a) indicates dust transport to the northwest Australian shelf from the continental interior (Figure S1f). Today, highest Th/K in the region is associated with the modern dust pathway (Figure S7). Furthermore, U ppm, which is also associated with heavy minerals (Text S2), shows similar variations as Th/K, exhibiting a large increase at the onset of the Arid Interval (Figure 2b). Uranium-bearing igneous rocks are exposed at the surface on the Australian continent [*Schofield*, 2009] and U ppm and Th/K are both elevated under the modern dust pathway (Figures S7 and S8). Although U is not a traditional paleoclimate proxy for dust transport, given the similarities with the %K and Th/K records, we suggest that at Site U1463, U can be used as a proxy for aridity in this region.

4. Discussion

4.1. Humidity, ETP, and Seasonality

Our records reveal the onset of widespread wet conditions across northwest Australia at ~5.5 Ma, lasting for 2.2 million years, indicated by high K, low-amplitude Th/K variation, and low U concentrations (Figure 2). Previous studies argued for a dry early Pliocene based on evidence showing the termination of Western Australia paleorivers in the middle Miocene [*Martin*, 2006]. Instead, we find that the early Pliocene was a time of rejuvenation of fluvial activity. The Humid Interval (~5.5 to 3.3 Ma) correlates with high %K and illite (Figures 2 and S5). Mass accumulation rates (Figure S5) do not increase markedly at the 5.5 Ma onset and instead decrease into the Humid Interval, indicating that %K is not an artifact of sediment accumulation rate and supporting our interpretation of %K as an indicator for precipitation and humidity.

Precipitation during the Humid Interval was likely year-round as evidenced by the low variability in Th/K; the negative correlation between the austral eccentricity-tilt-precession composite (ETP) and Th/K indicates that summer precipitation was enhanced during summer insolation maxima (Figure 2). Existing Australian paleoclimate records are heavily biased toward the southeast (Figure 3); thus, our new record fills a gap westward of the arid center, showing that while humidity decreased in the central region (d) wetter climates prevailed around the continental margin (Figures 3c and 3e) [*Martin*, 2006; *Metzger and Retallack*, 2010; *Miller et al.*, 2012]. Previous studies have assumed modern day climate gradients prevailed in the past, yet our data point to greater complexity and changing precipitation gradients over the past 6 million years. Humidity reduced gradually during the Transitional Interval from 3.3 to ~2.4 Ma (Figures 2 and 3b), concurrent with change from the climatically stable Humid Interval to a drier and more variable climate (Figure 2a). Increasing variability in Th/K, coupled with low K and high U concentrations, indicates that the continental interior became progressively more dry at ~2.4 Ma and heralded the onset of the Arid Interval (~2.4 Ma to at least 1 Ma).

During the Arid Interval, when the modern northwest dust pathway [*Bowler*, 1982] (Figures 2a and 2b) and the modern-like Australian monsoon became established, high Th/K ratios correlate with ETP maxima, indicating orbital configurations that favored strong seasonality. At ETP maxima, winds were sufficient for eolian sediment transport (with more variable Th/K and high U) to the study area. Conversely, at ETP minima during the Arid Interval, the seasonal insolation cycle was dampened, limiting eolian sediment supply. Thus, this major change in the Arid Interval, setting up the present-day climate pattern in northwest Australia, began at ~2.4 Ma, well after the intensification of Northern Hemisphere glaciation at 2.73 Ma [*Haug et al.*, 1999].

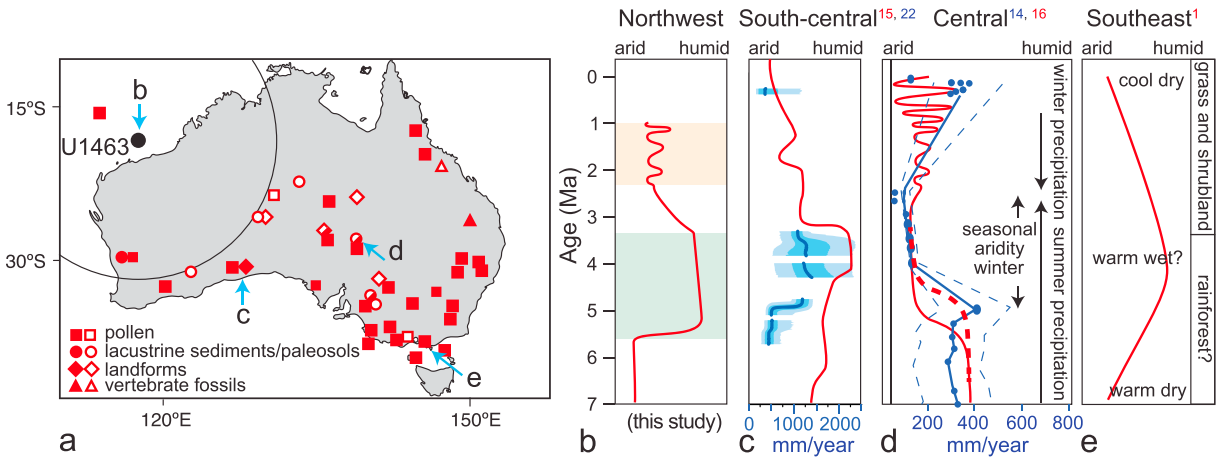

Figure 3. Compilation of Australian Neogene climate records and their proximity to Site U1463. (a) Map of the most important records (details in Text S4 and Figure S9). Open symbols represent early and middle Pleistocene (>0.7 Ma), and solid symbols indicate Pliocene records. Circle has a 1500 km radius. (b–e) Schematic interpretations of aridity records (blue arrows in Figure 3a) in northwest Australia (Figure 3b) (Site U1463, this study); south-central Australia (Figure 3c) [*Miller et al.*, 2012], including paleoprecipitation [*Sniderman et al.*, 2016]; central Australia (Figure 3d) [*Bowler*, 1982] with paleoprecipitation history [*Metzger and Retallack*, 2010]; solid and dashed red lines indicate range of timing; southeast Australia (Figure 3e) [*Martin*, 2006]. Figure 3c is a smoothed version of the original [*Miller et al.*, 2012] with blue precipitation records [*Sniderman et al.*, 2016] superimposed. Note arid and humid are relative terms and cannot be directly compared between panels.

4.2. Rapid Onset of Humidity at 5.5 Ma

A strong relationship exists between modern Australian climate and sea surface temperatures (SSTs) in the surrounding oceans [*King et al.*, 2014]. The onset of the Humid Interval occurred when the Western Pacific Warm Pool (WPWP) expanded west to the South China Sea [*Zhang et al.*, 2014; *Brierley et al.*, 2009] and eastern Indian Ocean [*Karas et al.*, 2011b]. This marks the end of global cooling in the late Miocene [*Herbert et al.*, 2016]. Warmer waters surrounding the Australian continent provided the increased moisture supply needed for the development and persistence of the Humid Interval (Figures 1d and 4). The presence of a tropical Pacific zonal SST gradient [*Zhang et al.*, 2014], which would have focused rainfall over the west Pacific, supports enhanced moisture availability in northern Australia. Concurrently, low levels of dust transport during the Humid Interval hint at the presence of greater vegetation cover in central Australia. Vegetation has a positive feedback on northern Australian rainfall when it is not seasonal [*Herold et al.*, 2011], enhancing available humidity. Indeed, the correlation between ETP and Th/K suggests low seasonality from 5.5 to 3.3 Ma (Figure 2a). A wet northwest Australia is consistent with evidence of a humid continental perimeter during the Pliocene [*Martin*, 2006; *Metzger and Retallack*, 2010; *Miller et al.*, 2012; *Sniderman et al.*, 2016] (Figures 3 and S9), and in agreement with high SST (Figure 4) at our study area.

4.3. Maritime Continent Control on Indian Ocean Circulation

Indian Ocean circulation was defined by a single dominant gyre from 5.5 to 3.3 Ma as indicated by warm western, central, and eastern Indian Ocean SSTs during the Humid Interval. The more open ITF transport limited development of robust equatorial circulation, aided by the more southerly Pliocene position of the Indian plate. Lower SSTs in the central and eastern Indian Ocean during the Transitional Interval (Figure 4) signal the start of more complex equatorial current systems. We suggest that the start of bigyral Indian Ocean circulation is the result of strengthening global atmospheric circulation [*Lawrence et al.*, 2013], combined with restriction of the ITF surface water transport [*Karas et al.*, 2011b] (Figure 1c). Models show reduced ITF transport drives enhanced precipitation in the western Pacific at the expense of the eastern Indian Ocean and northwest Australia, leading to a warmer and drier northwest Australia [*Krebs et al.*, 2011]. It was not until ~2.4 Ma, coincident with the onset of the Arid Interval, when modern, seasonally controlled equatorial circulation fully developed. As trade winds shifted equatorward, and global atmospheric circulation achieved a more modern position by ~2 Ma [*Lawrence et al.*, 2013], seasonality and equatorial Indian Ocean circulation were enhanced during the Arid Interval, along with offshore dust transport (Figure 1b).

Reduced moisture availability associated with the Transition Interval beginning at 3.3 Ma coincides with cooling in the WPWP [*Zhang et al.*, 2014], contracting global atmospheric circulation [*Lawrence et al.*, 2013], and

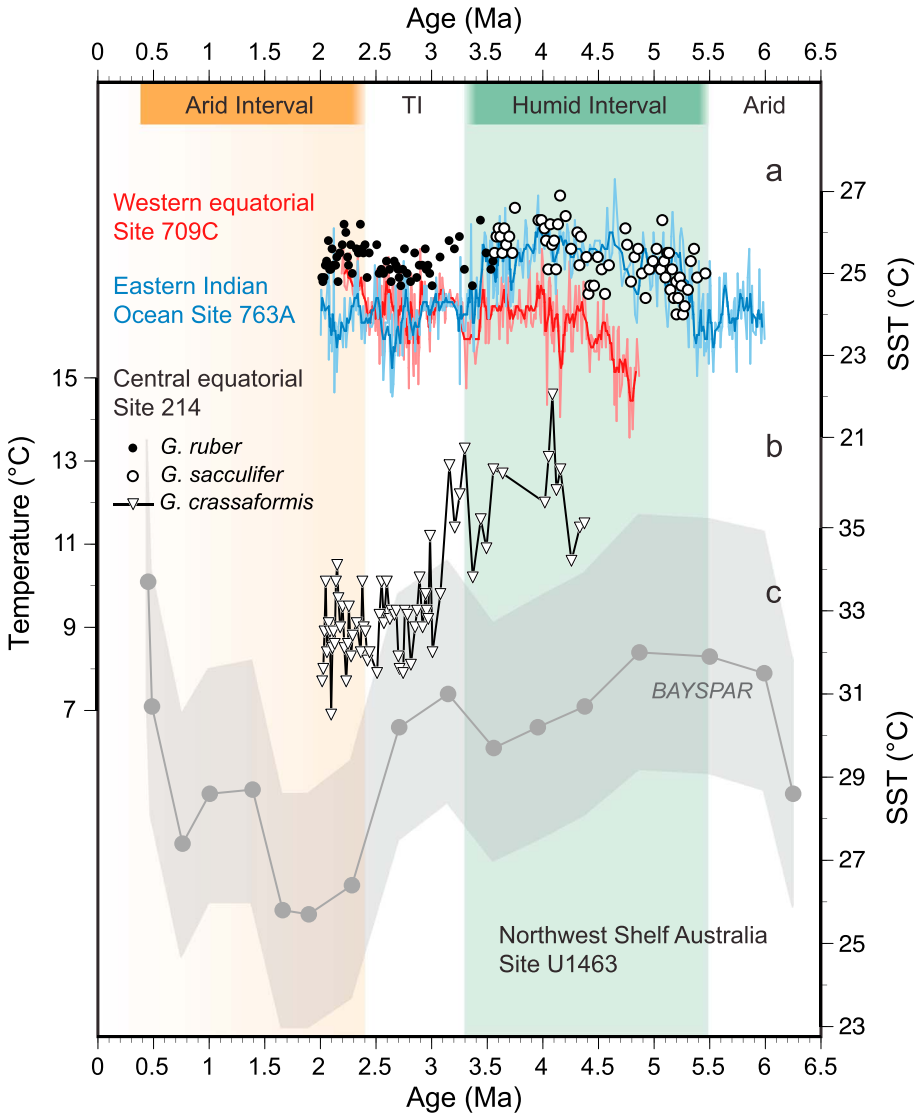

Figure 4. Sea surface temperature evolution in the Indian Ocean from 6 to 0.5 Ma. (a, b) Foraminiferal Mg/Ca-based temperatures from Western Equatorial Indian Ocean (Site 709 [*Karas et al.*, 2011b]) (red); Eastern Indian Ocean (Site 763A [*Karas et al.*, 2011b]) (blue; as in Figure 2), and Central Equatorial Indian Ocean (Site 214 [*Karas et al.*, 2009]) (black symbols)—where Figure 4a surface dwelling and Figure 4b deeper-dwelling planktonic foraminifer species reveal stable surface, and cooling deeper waters in the Central Equatorial Indian Ocean. Lines in Figure 4a are 5-point moving averages. Shaded green area indicates the Humid Interval (~5.5–3.3 Ma). (c) Low-resolution TEX_{86} data for Site U1463 plotted using Bayesian, Spatially-Varying Regression (BAYSPAR) calibration of *Tierney and Tingley* [2014], gray shading represents the 1-sigma error. We stress relative temperature changes and trends over time rather than absolute SST estimates.

decreased midlatitude and subpolar SSTs [*Karas et al.*, 2011a] (Figure 4). Central Indian Ocean sea surface conditions remained stable, whereas subsurface waters freshened and cooled between 3.5 and 2.95 Ma [*Karas et al.*, 2009, 2011b] associated with the ongoing ITF constriction. Specifically, eastern Indian Ocean SSTs dropped by 2–3°C from 3.3 Ma onward as the result of a reduction in surface ITF flow [*Karas et al.*, 2011b]. Coincident with the onset of the Arid Interval, an ~2°C cooling is recorded in the central Indian Ocean [*Herbert et al.*, 2010], full seasonality developed off Sumatra [*Gupta and Thomas*, 2003], benthic productivity increased in the eastern Indian Ocean [*Rai and Singh*, 2001], and drying in northeast Africa [*Liddy et al.*, 2016]. Our well log data document a tight connection between the timing of changes in Indian Ocean circulation and Australian climate (Figures 2 and 4). SST estimates at Site U1463 support this relationship, showing cooling into the Arid Interval (Figures 4 and S10).

5. Conclusions

The ongoing restriction of the ITF caused progressive oceanographic changes that likely drove shifts in precipitation. We attribute the correlation between ocean circulation and Australian climate to a combination and cumulative impact of tectonic changes and associated nonlinear climate feedbacks. It is becoming increasingly clear that the Indian Ocean plays an important role in global circulation and heat transport [*Schott et al.*, 2009; *Lee et al.*, 2015]. The major steps in reorganization of Indian Ocean circulation and Australian climate systems occurred at ~5.5 Ma, ~3.3 Ma, and ~2.4 Ma and do not coincide with the onset of Northern Hemisphere glaciation at ~2.73 Ma [*Haug et al.*, 1999]. We hypothesize that global climate may operate as two distinct but connected systems, one more closely associated with monsoons and the other with glaciation, with the Maritime Continent operating as a switchboard [*Cane and Molnar*, 2001; *Molnar and Cronin*, 2015]. East Africa, South Asia, and Western Australia appear to be predominantly influenced by the Indian Ocean [*Schott et al.*, 2009; *Fitzsimmons et al.*, 2013], whereas climates around the Pacific and Atlantic Oceans are more directly controlled by Northern Hemisphere glaciations [*Haug et al.*, 1999]. We suggest both climate systems are linked by the Maritime Continent. Similarly, some studies show that a shift from warmer south Pacific to cooler north Pacific waters, associated with ongoing tectonic reorganization in the Maritime Continent, contributed to Pliocene aridification in East Africa [*Cane and Molnar*, 2001; *Karas et al.*, 2009; *Liddy et al.*, 2016]. Recently, *Molnar and Cronin* [2015] hypothesized that emergence of the Maritime Continent strengthened tropical atmospheric Walker circulation to foster an estimated 0.7°C increase in the zonal SST gradient in the equatorial Pacific. Our records indicate that as Australia moved north, it directly influenced regional and global climate through gradual tectonic uplift of the Maritime Continent. The associated constriction of the ITF in turn impacted Australian climate and global ocean circulation. It thus appears that Australia as it collided with the Maritime Continent became an increasingly important driver of regional and global climate. Progressive constriction of the ITF during the Pliocene Humid Interval shifted control over the northwest Australian climate away from the Pacific, toward the Indian Ocean during the Arid Interval and modern times.

Appendix A

A1. Author Contributions

B.C. coordinated the writing effort; W.R. and J.H. were the primary coauthors and drafted most figures. D.D.V., J.H., and J.G. developed the age model. I.C. generated SST data. L.R. generated XRD data. W.R., J.H., W.R., D.D.V., G.A., L.R., J.G., I.C., T.I., K.B., C.M.M., S.G., and C.F. contributed to discussions and edited drafts. All coauthors were participants on IODP Expedition 356 and participated in generating the data published herein and shipboard data analysis.

A2. Additional IODP Expedition 356 Scientists (https://iodp.tamu.edu/scienceops/precruise/indonesianthruflow/participants.html)

B. L. Mamo[1], M. A. Kominz[2], H. V. McGregor[3], B. F. Petrick[4], H. Takayanagi[5], E. Levin[6], C. A. Korpanty[7], D. C. Potts[8], S. Baranwal[9,10], D. R. Franco[11], M. Gurnis[12], C. Haller[13], Y. He[14], T. Himmler[15], H. Iwatani[16], R. S. Jatiningrum[17], E. Y. Lee[18], A. Rastigar[19], and W. Zhang[20]

[1]School of Biological Sciences, University of Hong Kong, Hong Kong [2]Department of Geosciences, Western Michigan University, Kalamazoo, Michigan, USA [3]School of Earth and Environmental Sciences, University of Wollongong, Wollongong, NSW, Australia [4]Max Planck Institute for Chemistry, Mainz, Germany [5]Institute of Geology and Paleontology, Tohoku University, Sendai, Japan [6]Department of Earth and Planetary Sciences, University of California, Davis, California, USA [7]School of Biological Sciences, University of Queensland, Brisbane, Qld, Australia [8]Ecology and Evolutionary Biology and Institute of Marine Sciences, University of California, Santa Cruz, California, USA [9]Geological Survey of Norway, Trondheim, Norway [10]Centre for Arctic Gas Hydrate, Environment and Climate, Tromsø, Norway [11]Department of Geophysics, National Observatory, Rio de Janeiro, Brazil [12]Division of Geological and Planetary Sciences, California Institute of Technology, Pasadena, California, USA [13]College of Marine Science, University of South Florida, St. Petersburg, Florida, USA [14]Earth Sciences, Zhejiang University, Hangzhou, China [15]MARUM-Center for Marine and Environmental Sciences, Department of Geosciences, University of Bremen, Bremen, Germany

[16]School of Biological Sciences, University of Hong Kong, Hong Kong [17]Geoscience, Geotechnology and Material Resource Engineering, Akita University, Akita, Japan [18]Department of Geodynamics and Sedimentology, University of Vienna, Vienna, Austria [19]School of Applied Geology, Curtin University, Mounty Hawthorn, WA, Australia [20]MOE Key Laboratory of Surficial Geochemistry, Department of Earth Sciences, Nanjing University, Nanjing, China

Acknowledgments
This research used samples and data provided by the International Ocean Discovery Program. We thank the JRSO staff and the SIEM Offshore crew for their invaluable assistance and skill during the Expedition. We gratefully acknowledge the drilling proposal proponents and B. Wygal and N. McGee for graphic assistance. All data generated during IODP Expedition 356 are publicly accessible via the IODP-JOIDES Resolution Science Operator website (www.iodp.tamu.edu). We acknowledge financial support by the United States Science Support Program (to B.C., I.S.C., K.B., C.M.M., and C.S.F., National Science Foundation prime award OCE-1450528), the Naturalis Biodiversity Center (to W.R.), the Swedish Research Council (VR grants 2011-4866 and 2016-04434 to J.H.), the Deutsche Forschungsgemeinschaft (Projects VL 96/1-1 to D.D.V. and GR 3528/3-1 to J.G.), and the Australian Research Council (award to S.J.G.).

References

Bint, A. N. (1981), An early Pliocene pollen assemblage from Lake Tay, south-western Australia, and its phytogeographic implications, *Aus. J. Bot.*, *29*(3), 277–291.

Bowler, J. M. (1976), Aridity in Australia: Age, origins and expressions in aeolian landforms and sediments, *Earth Sci. Rev.*, *12*, 279–310, doi:10.1016/0012-8252(76)90008-8.

Bowler, J. M. (1982), Aridity in the late Tertiary and Quaternary of Australia, in *Evolution of the Flora and Fauna of Arid Australia*, edited by W. R. Barker and P. J. M. Greenslade, pp. 35–45, Peacock Publications, Adelaide, Australia.

Brierley, C. M., A. V. Fedorov, Z. Liu, T. D. Herbert, K. T. Lawrence, and J. P. LaRiviere (2009), Greatly expanded tropical warm pool and weakened Hadley circulation in the early Pliocene, *Science*, *323*(5922), 1714–1718, doi:10.1126/science.1167625.

Byrne, M., et al. (2008), Birth of a biome: Insights into the assembly and maintenance of the Australian arid zone biota, *Mol. Ecol.*, *17*, 4398–4417.

Byrne, M., et al. (2011), Decline of a biome: Evolution, contraction, fragmentation, extinction and invasion of the Australian mesic zone biota, *J. Biogeogr.*, *38*, 1635–1656.

Cane, M. A., and P. Molnar (2001), Closing of the Indonesian seaway as a precursor to east African aridification around 3–4 million years ago, *Nature*, *411*, 157–162, doi:10.1038/35075500.

Calvert, S. E., and T. F. Peterson (2007), Elemental proxies for palaeoclimatic and palaeoceanographic variability in marine sediments: Interpretation and application, *Dev. Mar. Geol.*, doi:10.1016/S1572-5480(07)01019-6.

Chen, X. Y., and C. E. Barton (1991), Onset of aridity and dune-building in central Australia: Sedimentological and magnetostratigraphic evidence from Lake Amadeus, *Palaeogeogr. Palaeoclimatol. Palaeoecol.*, *84*(1–4), 55–73, doi:10.1016/0031-0182(91)90035-P.

CSIRO and Bureau of Meteorology (2015), Climate change in Australia information for Australia's natural resource management regions: Technical Report, CSIRO and Bureau of Meteorology, Australia.

Dodson, J. R., and A. Ramrath (2001), An upper Pliocene lacustrine environmental record from south-western Australia—Preliminary results, *Palaeogeogr. Palaeoclimatol. Palaeoecol.*, *167*(3–4), 309–320, doi:10.1016/S0031-0182(00)00244-3.

De Vleeschouwer, D., et al. (2017), Quantifying K, U, and Th contents of marine sediments using shipboard natural gamma radiation spectra measured on DV JOIDES Resolution, *Geochem. Geophys. Geosyst.*, *18*, 1053–1064, doi:10.1002/2016GC006715.

Du, Y., and T. Qu (2010), Three inflow pathways of the Indonesian Throughflow as seen from the simple ocean data assimilation, *Dyn. Atmos. Ocean.*, *50*(2), 233–256, doi:10.1016/j.dynatmoce.2010.04.001.

Ehrenberg, S. N., and T. A. Svånå (2001), Use of spectral gamma-ray signature to interpret stratigraphic surfaces in carbonate strata: An example from the Finnmark carbonate platform (Carboniferous-Permian), Barents Sea, *Am. Assoc. Pet. Geol. Bull.*, *85*(2), 295–308, doi:10.1016/0025-326X(78)90448-4.

English, P., N. A. Spooner, J. Chappell, D. G. Questiaux, and N. G. Hill (2001), Lake Lewis basin, central Australia: Environmental evolution and OSL chronology, *Quat. Int.*, *83*, 81–101.

Fitzsimmons, K. E., et al. (2013), Late Quaternary palaeoenvironmental change in the Australian drylands, *Quat. Sci. Rev.*, *74*, 78–96, doi:10.1016/j.quascirev.2012.09.007.

Fujioka, T., and J. Chappell (2010), History of Australian aridity: Chronology in the evolution of arid landscapes, *Geol. Soc. London, Spec. Publ.*, *346*(1), 121–139, doi:10.1144/SP346.8.

Fujioka, T., J. Chappell, M. Honda, I. Yatsevich, K. Fifield, and D. Fabel (2005), Global cooling intiated stony deserts in central Australia 2–4 Ma, dated by cosmogenic ^{21}Ne-^{10}Be, *Geology*, *33*(12), 993–996, doi:10.1130/G21746.1.

Gallagher, S. J., et al. (2017), Expedition 356 methods, in *Indonesian Throughflow*, Proceedings of the International Ocean Discovery Program, vol. 356, edited by S. J. Gallagher et al., International Ocean Discovery Program, College Station, Tex., doi:10.14379/iodp.proc.356.102.2017.

Geoscience Australia (2015), Radmap unfiltered ppm Uranium v3. [Available at http://www.ga.gov.au/. Commonwealth of Australia.]

Gingele, F. X., and P. De Deckker (2004), Fingerprinting Australia's rivers with clay minerals and the application for the marine record of climate change, *Aust. J. Earth Sci.*, *51*(3), 339–348, doi:10.1111/j.1400-0952.2004.01061.x.

Gingele, F. X., P. De Deckker, and C.-D. Hillenbrand (2001a), Clay mineral distribution in surface sediments between Indonesia and NW Australia—Source and transport by ocean currents, *Mar. Geol.*, *179*, 135–146.

Gingele, F. X., P. De Deckker, and C. D. Hillenbrand (2001b), Late quaternary fluctuations of the leeuwin current and palaeoclimates on the adjacent land masses: Clay mineral evidence, *Aust. J. Earth Sci.*, *48*(6), 867–874, doi:10.1046/j.1440-0952.2001.00905.x.

Gordon, A. L. (2005), Oceanography of the Indonesian seas and their throughflow, *Oceanography*, *18*(4), 14–27, doi:10.5670/oceanog.2005.18.

Gradstein, F. M., J. G. Ogg, M. D. Schmitz, G. M. Ogg (2012), The geologic time scale 2012, Elsevier, Amsterdam.

Groeneveld, J., et al. (2017), Australian shelf sediments reveal shifts in Miocene Southern Hemisphere Westerlies, *Sci. Adv.*, doi:10.1126/sciadv.1602567.

Gupta, A. K., and E. Thomas (2003), Initiation of Northern Hemisphere glaciation and strengthening of the northeast Indian monsoon: Ocean drilling program site 758, eastern equatorial Indian Ocean, *Geology*, *31*(1), 47, doi:10.1130/0091-7613(2003)031<0047:IONHGA>2.0.CO;2.

Hall, R. (2012), Sundaland and Wallacea: Geology, plate tectonics and palaeogeography, in *Biotic Evolution and Environmental Change in Southeast Asia*, edited by D. J. Gower et al., pp. 32–78, Cambridge Univ. Press, New York.

Haug, G. H., D. M. Sigman, R. Tiedemann, T. F. Pedersen, and M. Sarnthein (1999), Onset of permanent stratification in the subarctic Pacific Ocean, *Nature*, *401*(6755), 21–24, doi:10.1038/44550.

Herbert, T., D. Herbert, L. C. Peterson, K. T. Lawrence, and Z. Liu (2010), Tropical ocean temperatures over the past 3.5 million years, *Science*, *328*, 1530–1535.

Herbert, T. D., K. T. Lawrence, A. Tzanova, L. C. Peterson, R. Caballero-Gill, and C. S. Kelly (2016), Late Miocene global cooling and the rise of modern ecosystems, *Nat. Geosci.*, *9*(11), 843–847.

Herold, N., M. Huber, D. R. Greenwood, R. D. Müller, and M. Seton (2011), Early to middle Miocene monsoon climate in Australia, *Geology*, *39*(1), 3–6, doi:10.1130/G31208.1.

Hesselbo, S. P. (1996), Spectral gamma-ray logs in relation to clay mineralogy and sequence stratigraphy, Cenozoic of the Atlantic margin, offshore New Jersey 1 relationship of spectral gamma-ray units to depositional geometry, *Proc. Ocean Drill. Progam, Sci. Results*, *150*, 411–422.

Hill, R. S. (2004), Origins of the southeastern Australian vegetation, *Philos. Trans. R. Soc. London, Ser. B*, *359*(1450), 1537–1549, doi:10.1098/rstb.2004.1526.

Hocknull, S. A., J. X. Zhao, Y. X. Feng, and G. E. Webb (2007), Responses of middle Pleistocene rainforest vertebrates to climate change in Australia, *Earth Planet. Sci. Lett.*, *264*, 317–331, doi:10.1016/j.epsl.2007.10.004.

Holper, P. (2011), Climate change science information paper: Australian rainfall—Past, present and future, Australian Climate Change Science Information Program. [Available at http://www.cawcr.gov.au/publications/otherreports/rainfall.pdf.]

Hope, P., B. Timbal, and R. Fawcett (2010), Associations between rainfall variability in the southwest and southeast of Australia and their evolution through time, *Int. J. Climatol.*, *30*(9), 1360–1371, doi:10.1002/joc.1964.

Hopmans, E. C., S. Schouten, R. D. Pancost, M. T. J. Van Der Meer, and J. S. Sinninghe Damsté (2000), Analysis of intact tetraether lipids in archaeal cell material and sediments by high performance liquid chromatography/atmospheric pressure chemical ionization mass spectrometry, *Rapid Commun. Mass Spectrom.*, *14*(7), 585–589, doi:10.1002/(SICI)1097-0231(20000415)14:7<585::AID-RCM913>3.0.CO;2-N.

Hopmans, E. C., J. W. H. Weijers, E. Schefuß, L. Herfort, J. S. Sinninghe Damsté, and S. Schouten (2004), A novel proxy for terrestrial organic matter in sediments based on branched and isoprenoid tetraether lipids, *Earth Planet. Sci. Lett.*, *224*(1–2), 107–116, doi:10.1016/j.epsl.2004.05.012.

Imbrie, J. (1985), A theoretical framework for the Pleistocene ice ages, *J. Geol. Soc. London*, *142*(3), 417–432, doi:10.1144/gsjgs.142.3.0417.

Karas, C., D. Nürnberg, A. K. Gupta, R. Tiedemann, K. Mohan, and T. Bickert (2009), Mid-Pliocene climate change amplified by a switch in Indonesian subsurface throughflow, *Nat. Geosci.*, *2*(6), 434–438, doi:10.1038/ngeo520.

Karas, C., D. Nürnberg, R. Tiedemann, and D. Garbe-Schönberg (2011a), Pliocene climate change of the Southwest Pacific and the impact of ocean gateways, *Earth Planet. Sci. Lett.*, *301*(1–2), 117–124, doi:10.1016/j.epsl.2010.10.028.

Karas, C., D. Nürnberg, R. Tiedemann, and D. Garbe-Schönberg (2011b), Pliocene Indonesian Throughflow and Leeuwin Current dynamics: Implications for Indian Ocean polar heat flux, *Paleoceanography*, *26*, 1–9, doi:10.1029/2010PA001949.

Kershaw, A. P., H. A. Martin, and JRC McEwen Mason (1994), The Neogene: A period of transition, in *History of the Australian Vegetation: Cretaceous to Recent*, edited by R. S. Hill, pp. 299–327, Cambridge Univ. Press, Cambridge, Mass.

Kim, J. H., J. van der Meer, S. Schouten, P. Helmke, V. Willmott, F. Sangiorgi, N. Koç, E. C. Hopmans, and J. S. S. Damsté (2010), New indices and calibrations derived from the distribution of crenarchaeal isoprenoid tetraether lipids: Implications for past sea surface temperature reconstructions, *Geochim. Cosmochim. Acta*, *74*(16), 4639–4654, doi:10.1016/j.gca.2010.05.027.

King, A. D., M. G. Donat, L. V. Alexander, and D. J. Karoly (2014), The ENSO-Australian rainfall teleconnection in reanalysis and CMIP5, *Clim. Dyn.*, 2623–2635, doi:10.1007/s00382-014-2159-8.

Krebs, U., W. Park, and B. Schneider (2011), Pliocene aridification of Australia caused by tectonically induced weakening of the Indonesian throughflow, *Palaeogeogr. Palaeoclimatol. Palaeoecol.*, *309*(1–2), 111–117, doi:10.1016/j.palaeo.2011.06.002.

Kuhnt, W., A. Holbourn, J. Xu, B. Opdyke, P. De Deckker, U. Röhl, and M. Mudelsee (2015), Southern Hemisphere control on Australian monsoon variability during the late deglaciation and Holocene, *Nat. Commun.*, *6*, 5916, doi:10.1038/ncomms6916.

Laskar, J., A. Fienga, M. Gastineau, and H. Manche (2011), La2010: A new orbital solution for the long term motion of the Earth, *Astron. Astrophys.*, *4*, 17, doi:10.1051/0004-6361/201116836.

Lawrence, K. T., D. M. Sigman, T. D. Herbert, C. A. Riihimaki, C. T. Bolton, A. Martinez-Garcia, A. Rosell-Mele, and G. H. Haug (2013), Time-transgressive North Atlantic productivity changes upon Northern Hemisphere glaciation, *Paleoceanography*, *28*, 740–751, doi:10.1002/2013PA002546.

Lee, S.-K., W. Park, M. O. Baringer, A. L. Gordon, B. Huber, and Y. Liu (2015), Pacific origin of the abrupt increase in Indian Ocean heat content during the warming hiatus, *Nat. Geosci.*, *8*(May), 445–449, doi:10.1038/ngeo2438.

Liddy, H. M., S. J. Feakins, and J. E. Tierney (2016), Cooling and drying in northeast Africa across the Pliocene, *Earth Planet. Sci. Lett.*, *449*, 430–438.

Lisiecki, L. E., and M. E. Raymo (2005), A Pliocene-Pleistocene stack of 57 globally distributed benthic $\delta^{18}O$ records, *Paleoceanography*, *20*, PA1003, doi:10.1029/2004PA001071.

Longo, W. M., J. T. Dillon, R. Tarozo, J. M. Salacup, and Y. Huang (2013), Unprecedented separation of long chain alkenones from gas chromatography with a poly(trifluoropropylmethylsiloxane) stationary phase, *Org. Geochem.*, *65*, 94–102, doi:10.1016/j.orggeochem.2013.10.011.

Macphail, M. K. (1997), Late neogene climates in Australia: Fossil pollen- and spore-based estimates in retrospect and prospect, *Aust. J. Bot.*, *45*(3), 425–464, doi:10.1071/BT96052.

Macphail, M. K. (2007), Australian Palaeoclimates: Cretaceous to Tertiary—A review of palaeobotanical and related evidence to the year 2000. CRC LEME Open File Report 151 (Cooperative Research Centre for Landscape Environments and Mineral Exploration, Bentley, Australia).

Manheim, F. T., and F. L. Sayles (1974), Composition and origin of interstitial waters of marine sediments based on deep sea drill cores, in *The Sea*, edited by E. D. Goldberg, vol. 5, pp. 527–568, Wiley, New York.

Martin, H. A., and A. McMinn (1993), Palynology of sites 815 and 823: The Neogene vegetation history of coastal north-eastern Australia, Proceedings of the Ocean Drilling Program, *Sci. Results*, *133*, 115–123.

Martin, H. A., and A. McMinn (1994), Late Cainozoic vegetation history of North-western Australia, from the Palynology of a Deep Sea Core (ODP Site 765), *Aus. J. Bot.*, *42*, 95–102.

Martin, H. A. (2006), Cenozoic climatic change and the development of the arid vegetation in Australia, *J. Arid Environ.*, *66*(3 SPEC. ISS), 533–563, doi:10.1016/j.jaridenv.2006.01.009.

McLaren, S., and M. W. Wallace (2010), Plio-Pleistocene climate change and the onset of aridity in southeastern Australia, *Global Planet. Change*, *71*(1–2), 55–72, doi:10.1016/j.gloplacha.2009.12.007.

Metzger, C. A., and G. J. Retallack (2010), Paleosol record of Neogene climate change in the Australian outback, *Aust. J. Earth Sci.*, *57*(7), 871–885, doi:10.1080/08120099.2010.510578.

Meyers, S. R. (2014), Astrochron: An R package for astrochronology (Version 0.4.1). [Available at http://www.geology.wisc.edu/~smeyers.]

Miller, C. R., N. P. James, and Y. Bone (2012), Prolonged carbonate diagenesis under an evolving late Cenozoic climate; Nullarbor Plain, southern Australia, *Sediment. Geol.*, *261–262*, 33–49, doi:10.1016/j.sedgeo.2012.03.002.

Molnar, P., and T. W. Cronin (2015), Growth of the Maritime Continent and its possible contribution to recurring ice ages, *Paleoceanography*, *30*, 196–225, doi:10.1002/2014PA002752.

Montanari, S., J. Louys, and G. J. Price (2013), Pliocene Paleoenvironments of southeastern Queensland, Australia inferred from stable isotopes of marsupial tooth enamel, *PLoS One*, *8*(6), doi:10.1371/journal.pone.0066221.

Nakamura, A., and P. R. Milligan (2015), Radiometric map of Australia (third edition), scale 1:15 000 000, Geoscience Australia, Canberra. [Available at http://www.ga.gov.au/metadata-gateway/metadata/record/82883/.]

Nicholson, S. (2011), *Dryland Climatology*, Cambridge Univ. Press, Cambridge, New York.

O'Hara, M. J., N. Fry, and H. M. Prichard (2001), Minor phases as carriers of trace elements in non-modal crystal-liquid separation processes II: Illustrations and bearing on behaviour of REE, U, Th and the PGE in igneous processes, *J. Petrol.*, *42*(10), 1887–1910, doi:10.1093/petrology/42.10.1887.

Quilty, P. G. (1994), The background: 144 million years of Australian palaeoclimate and palaeogeography, in *The History of the Australian Vegetation: Cretaceous to Recent*, edited by R. S. Hill, pp. 14–43, Cambridge Univ. Press, Cambridge, U. K.

Rai, A. K., and V. B. Singh (2001), Late neogene deep-sea benthic foraminifera at ODP site 762B, eastern Indian Ocean: Diversity trends and palaeoceanography, *Palaeogeogr. Palaeoclimatol. Palaeoecol.*, *173*(1–2), 1–8, doi:10.1016/S0031-0182(01)00299-1.

Schofield, A. (2009), Uranium Content of Igneous Rocks of Australia1:5000000 Maps—Explanatory Notes and Discussion, Record 2009/17, p. 20, Geoscience Australia, Canberra.

Schott, F. A., S.-P. Xie, and J. P. McCreary Jr (2009), Indian Ocean circulation and climate variability, *Rev. Geophys.*, *47*, RG1002, doi:10.1029/2007RG000245.1.

Schouten, S., E. C. Hopmans, E. Schefuß, and J. S. Sinninghe Damsté (2002), Distributional variations in marine crenarchaeotal membrane lipids: A new tool for reconstructing ancient sea water temperatures?, *Earth Planet. Sci. Lett.*, *204*(1–2), 265–274, doi:10.1016/S0012-821X(02)00979-2.

Šimíček, D., and O. Bábek (2015), Spectral gamma-ray logging of the Grès d'Annot, SE France: An outcrop analogue to geophysical facies mapping and well-log correlation of sand-rich turbidite reservoirs, *Mar. Pet. Geol.*, *60*, 1–17, doi:10.1016/j.marpetgeo.2014.10.010.

Sniderman, J. M. K. (2011), Early Pleistocene vegetation change in upland south-eastern Australia, *J. Biogeogr.*, *38*(8), 1456–1470, doi:10.1111/j.1365-2699.2011.02518.x.

Sniderman, J. M. K., B. Pillans, P. B. O'Sullivan, and A. P. Kershaw (2007), Climate and vegetation in southeastern Australia respond to Southern Hemisphere insolation forcing in the late Pliocene—Early Pleistocene, *Geology*, *35*(1), 41–44, doi:10.1130/G23247A.1.

Sniderman, J. M. K., G. J. Jordan, and R. M. Cowling (2013), Fossil evidence for a hyperdiverse sclerophyll flora under a non-Mediterranean-type climate, *Proc. Natl. Acad. Sci. U.S.A.*, *110*(9), 3423–3428, doi:10.1073/pnas.1216747110.

Sniderman, J. M. K., J. D. Woodhead, J. Hellstrom, G. J. Jordan, R. N. Drysdale, J. J. Tyler, and N. Porch (2016), Pliocene reversal of late Neogene aridification, *Proc. Natl. Acad. Sci. U.S.A.*, doi:10.1073/pnas.1520188113.

Steinke, S., M. Mohtadi, M. Prange, V. Varma, D. Pittauerova, and H. W. Fischer (2014), Mid- to late-Holocene Australian-Indonesian summer monsoon variability, *Quat. Sci. Rev.*, *93*, 142–154, doi:10.1016/j.quascirev.2014.04.006.

Stuut, J. B. W., F. Temmesfeld, and P. De Deckker (2014), A 550 ka record of aeolian activity near North West Cape, Australia: Inferences from grain-size distributions and bulk chemistry of SE Indian Ocean deep-sea sediments, *Quat. Sci. Rev.*, *83*, 83–94, doi:10.1016/j.quascirev.2013.11.003.

Suppiah, R. (1992), The Australian summer monsoon: A review, *Prog. Phys. Geogr.*, *40*(November), 283–318, doi:10.1177/030913339201600302.

Svendsen, J. B., and N. R. Hartley (2001), Comparison between outcrop-spectral gamma ray logging and whole rock geochemistry: Implications for quantitative reservoir characterisation in continental sequences, *Mar. Pet. Geol.*, *18*(6), 657–670, doi:10.1016/S0264-8172(01)00022-8.

Thomson, D. J. (1982), Spectrum estimation and harmonic analysis, *Proc. IEEE*, *70*(9), 1055–1096, doi:10.1109/PROC.1982.12433.

Tierney, J. E., and M. P. Tingley (2014), A Bayesian, spatially-varying calibration model for the TEX_{86} proxy, *Geochim. Cosmochim. Acta*, *127*, 83–106, doi:10.1016/j.gca.2013.11.026.

Tierney, J. E., and M. P. Tingley (2015), A TEX_{86} surface sediment database and extended Bayesian calibration, *Sci. Data*, *2*, 150029, doi:10.1038/sdata.2015.29.

Young, J. R. (1998), Neogene, in *Calcareous Nannofossil Biostratigraphy*, edited by P. Bown, pp. 2245–265, Cambridge Univ. Press, Cambridge, U. K.

Zhang, Y. G., M. Pagani, and Z. Liu (2014), A 12-million-year temperature history of the tropical Pacific Ocean, *Science*, *344*(6179), 84–87, doi:10.1126/science.1246172.

Zheng, H., K. H. Wyrwoll, Z. Li, and C. McA Powell (1998), Onset of aridity in southern Western Australia—A preliminary palaeomagnetic appraisal, *Global Planet. Change*, *18*(3–4), 175–187, doi:10.1016/S0921-8181(98)00019-8.

Zhisheng, A., J. M. Bowler, N. D. Opdyke, P. G. Macumber, and J. B. Firman (1986), Palaeomagnetic stratigraphy of Lake Bungunnia: Plio-pleistocene precursor of aridity in the murray basin, Southeastern Australia, *Palaeogeogr. Palaeoclimatol. Palaeoecol.*, *54*(1–4), 219–239, doi:10.1016/0031-0182(86)90126-4.